Nuclear Materials and Energy 24 (2020) 100772

Contents lists available at ScienceDirect

Nuclear Materials and Energy

journal homepage: www.elsevier.com/locate/nme

SANS and neutron diffraction study of ausformed EUROFER97/2 ferritic/martensitic steel

R. Coppola[a,*], A. Feoktystov[b], T. Mueller[b], L. Pilloni[c], A. Radulescu[b]

[a] ENEA-Casaccia, FSN-ING, Via Anguillarese 301, 00123 Roma, Italy
[b] Forschungszentrum Jülich GmbH, Jülich Centre for Neutron Science (JCNS) at Heinz Maier-Leibnitz Zentrum (MLZ), Lichtenbergstr. 1, 85748 Garching, Germany
[c] ENEA-Casaccia, SSTP-PROMAS-MATPRO, Via Anguillarese 301, 00123 Roma, Italy

ARTICLE INFO

Keywords:
Eurofer97
Ausforming
Small-angle neutron scattering
Neutron diffraction

ABSTRACT

Small-angle neutron scattering (SANS) and neutron diffraction have been utilized for micro-structural characterization of Eurofer97/2 heats submitted to thermo-mechanical treatments, with the aim to investigate macroscopic material volumes and to complete the local information provided by scanning electron microscopy. The measurements were carried out at MLZ in Garching, utilizing for SANS also a polarized neutron beam. The investigated samples had been submitted to austenitization and tempering at different temperatures, as well as to double austenitization and to "ausforming", that is austenitization followed by hot rolling. For most of the examined treatments, nearly identical SANS cross-sections were measured, close to the one of Eurofer97/1. In the ausformed sample the nuclear SANS cross-section is also nearly identical to the other samples but the magnetic one is one order of magnitude higher. Furthermore, over a wide experimental interval its nuclear-magnetic interference, measured by polarized SANS, is of opposite sign with respect to the non-ausformed samples. Neutron diffraction measurements provided strong evidence that the origin of such effects is due to the presence of the non-magnetic austenite phase in the ausformed sample, with an estimated volume fraction of 0.17 ± 0.02; within the experimental resolution, it disappears after subsequent tempering.

1. Introduction

Ferritic/martensitic steels currently appear as one of the most realistic options as structural materials for DEMO technology; however, high temperature mechanical properties, creep resistance in particular, need to be improved for optimizing in service behavior at 650 °C or at higher temperatures [1,2]. Within this frame, a series of innovative Eurofer97/2 heats has been developed; the most favorable elemental compositions and preliminary thermo-mechanical treatments have been systematically investigated [3–5]. Namely, with respect to Eurofer97/1 the C, W and N contents have been varied to different extents in the different heats, in order to reduce $M_{23}C_6$ precipitation, promote V-rich precipitation, contribute in optimizing grain size [3]. Optimization of the preliminary treatment concerned austenitization and tempering temperatures, the effect of a double austenitization and the effect of a combined thermo-mechanical treatment consisting in a short hot-rolling stage at 650 °C or 750 °C after austenitization. This treatment, usually referred to as "ausforming", is aimed to tune carbide precipitation in such a way to favor pinning of dislocations with beneficial effects on creep resistance [6–9]. The produced heats were mechanically characterized by fatigue and creep tests; their grain size micro-structure was investigated by scanning electron microscopy (SEM). Preliminary X-ray diffraction measurements were also carried out [10]. Promising results were obtained concerning creep resistance and impact properties, but no clear correlation could be established between the achieved improvements and the changes introduced in chemical composition and thermo-mechanical treatments. Consequently, small-angle neutron scattering (SANS) and neutron diffraction measurements were carried out on some of these samples in order to contribute in characterizing their micro-structure and trying to understand the effective role of the parameters selected for each heat. In fact, neutron beams can probe magnetic micro-structural features and allow for an investigation of massive samples, with typical volumes as large as 0.1 cm^3. Therefore, the obtained results can be more directly compared with those of mechanical testing and are in any case more representative of bulk properties of the investigated samples. These two techniques are also complementary to each other: SANS provides the distribution of defects, such as precipitates or micro-voids, while neutron diffraction allows to identify the crystallographic phases present after the different metallurgical treatments. The micro-structure of the

* Corresponding author.
E-mail address: roberto.coppola@enea.it (R. Coppola).

https://doi.org/10.1016/j.nme.2020.100772
Received 1 February 2020; Received in revised form 25 May 2020; Accepted 2 July 2020
Available online 08 July 2020

Table 1
Chemical composition of the investigated samples (wt%, Fe bal).

Sample	Cr	C	W	Ta	Mn	V	N
Eurofer97/1*	9	0.12	1.08	0.14	0.48	0.2	0.03
Eurofer97/2-2991 austenitization 1075 °C + ausforming at 650 °C	8.8	0.06	0.97	0.05	0.5	0.3	0.07
Eurofer97/2–2991 aust. 1075 °C + ausf. 650 °C + 1 h 760 °C	8.8	0.06	0.97	0.05	0.5	0.3	0.07
Eurofer97/2 – LT double aust. 980 °C + 760 °C 1 h	8.95	0.11	1.80	0.15	0.092	0	0.002

*Reference heat 83697, 1040 °C 30′ + 750 °C 1.5 h.

investigated materials is very complex and only a limited number of samples was investigated, namely only one ausformed sample. Therefore the results presented here below are not intended as a conclusive study, but as a first, necessary step to contribute in the metallurgical characterization of such Eurofer97/2 heats.

2. Material characterization

The most significant SANS and neutron diffraction effects were detected in the three Eurofer97/2 samples listed in Table 1. A sample of Eurofer97/1 submitted to standard treatment was also measured, both to check the changes associated to the different elemental compositions of the new heats and to compare with previous SANS measurements of this same sample [11]. SEM observations of these Eurofer97/2 samples are included in Ref. [3], showing grain size distribution and nitride precipitates. The samples utilized for the SANS measurements were prepared in the shape of rectangular platelets, approximately 1 cm × 1 cm × 0.7 mm in size. Each of them was cut from the original ingot, then its surfaces were mechanically polished to avoid spurious SANS effects. After ausforming, a grain texture with preferential direction is produced in the heats as a consequence of the hot rolling stage. In preparing the first samples for the SANS measurements it was not possible to cut all of them with the same orientation with respect to the rolling direction, therefore some uncertainties are present in the 2D SANS data, as discussed in Sec. 3 here below. Several other samples were investigated by SANS, submitted to double austenitization and to creep at 650 °C for 1650 h, under a load of 100 MPa: within the experimental uncertainties, no significant changes were observed among their respective SANS cross-sections and also comparing them to Eurfer97/1. The same samples utilized for the SANS measurements were utilized also for the neutron diffraction ones.

3. Experimental techniques

General information on the SANS technique is available in Refs. [12,13]; the scheme of one of the two utilized SANS instruments is shown in Fig. 1. For studying magnetic samples, an external magnetic field of at least 1 T must be applied to saturate their magnetization and measure the nuclear and the magnetic SANS components separately. In fact, for such samples the total SANS cross-section $d\Sigma(Q)/d\Omega$ (Ω stands for the solid angle) is

$$d\Sigma(Q)/d\Omega = d\Sigma(Q)/d\Omega_{nucl} + d\Sigma(Q)/d\Omega_{mag}\sin^2\alpha \quad (1)$$

where α is the azimutal angle on the detector plane. Parallel to the magnetic field ($\alpha = 0^\circ$) the nuclear SANS cross-section is measured, perpendicular to it ($\alpha = 90^\circ$) the sum of the nuclear and magnetic ones is measured; they are usually determined by selecting on the detector plane angular sectors 15° wide around these two directions. Their ratio $R(Q)$ (also defined "A" in the literature)

$$R(Q) = \frac{d\Sigma(Q)/d\Omega_{nucl} + d\Sigma(Q)/d\Omega_{mag}}{d\Sigma(Q)/d\Omega_{nucl}} = 1 + (\Delta\rho)^2_{mag}/(\Delta\rho)^2_{nucl} \quad (2)$$

is related to the composition of the micro-structural defects, $(\Delta\rho)^2$ being the "contrast" or square difference in neutron scattering length density (nuclear and magnetic respectively) between the observed nuclear and magnetic defects and the matrix.

A general introduction to polarized SANS can be found in Refs. [14,15]; applications of this technique to the study of ferritic/martensitic steels are presented in Refs. [16,17]. Polarized neutron beams are obtained utilizing magnetic super-mirrors placed before the sample and a spin flipper to reverse the direction of the neutron spin with respect to the applied magnetic field (Fig. 1). Defining the nuclear and the magnetic SANS cross-sections as $(d\Sigma(Q)/d\Omega)_{nucl} = N^2$ and $(d\Sigma(Q)/d\Omega)_{mag} = M^2$ respectively (with N and M scattering amplitudes), for a given angle α on the detector plane between the scattering vector Q and the magnetic field H, the cross sections measured in the spin directions parallel (+) and anti-parallel (−) to the applied magnetic field with polarization 100% can be written as:

$$(d\Sigma(Q)/d\Omega)_{\pm} = N^2 \pm 2NM\sin^2\alpha + M^2\sin^2\alpha \quad (3)$$

For $\alpha = 0^\circ$ N^2 is obtained. For $\alpha = 90^\circ$ the nuclear plus magnetic SANS component, $N^2 + M^2$, and the nuclear-magnetic interference term, NM, are obtained respectively as follows:

$$((d\Sigma(Q)/d\Omega)_+ + (d\Sigma(Q)/d\Omega)_-)/2 = N^2 + M^2 \quad (4)$$

$$((d\Sigma(Q)/d\Omega)_+ - (d\Sigma(Q)/d\Omega)_-)/2 = 2NM \quad (5)$$

Following Eq. (5), NM is proportional to $(\Delta\rho)_{mag}(\Delta\rho)_{nucl}$, therefore combining it with the measurement of $R(Q)$ in Eq. (2), more information can in principle be obtained on the composition of defects originating the measured SANS effects, as shown in the work of Ref. [16].

A first series of SANS measurements has been carried out utilizing the KWS-2 instrument [18]. Sample-to-detector distances D of 2 m and 8 m, with 5 Å neutron wavelength λ, and of 20 m, with 10 Å neutron wavelength, were selected: in the real space, that corresponds to an interval of observable defect sizes ranging approximately from 10 Å to 500 Å. An external 1.5 T magnetic field was applied. A second series of SANS measurements, including polarized SANS, was carried out at the KWS-1 instrument [19], utilizing the same D values, λ = 5 Å and applying an external magnetic field of 1.5 T. The polarization is changed by a radio-frequency spin-flipper (Fig. 1) covering the full bandwidth λ = 4.5 to 20 Å with polarization 90% – 95%. Calibration of the recorded neutron counts to physical units, in order to get the absolute values of SANS cross-sections, was obtained following the experimental protocols and related software available at these instruments [18,19].

The neutron diffraction measurements were carried out utilizing the DNS instrument [20]. A neutron wavelength λ = 2.1 Å was utilized and the investigated 2θ range was 5°–135°. This instrument is optimized for a high polarized flux, sacrificing resolution, due to the short flight path, focusing monochromator and the detector size (vertical 15 cm, horizontal 2.54 cm). The samples could not be measured at the same time but in different runs, during different reactor cycles and with different slit settings: therefore, although identical instrument parameters were selected, background levels were different in these different runs. The diffractograms of the measured samples were normalized for incoming neutron flux, and corrected for angular coverage and detector efficiency. However, given the restricted available Q range, a full refinement of the obtained data was not possible.

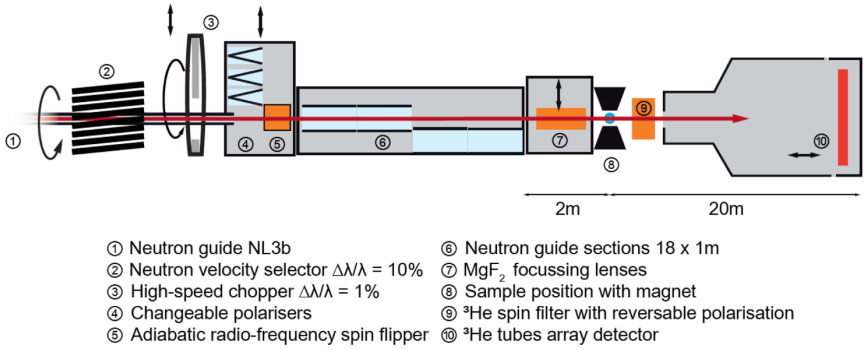

Fig. 1. Scheme of the KWS-1 SANS instrument at FRM II Garching. The long red arrow (1) represents the incoming neutron beam; polarisers (3) and spin-flipper (4) produce polarized neutron beam oriented either parallel or anti-parallel with respect to the vertical magnetic field (7) applied to the sample (blue spot). The picture is reproduced from Ref. [19], by kind authorization of the MLZ Users Office. (For interpretation of the references to colour in this figure legend, the reader is referred to the web version of this article.)

4. Results and discussion

In most of the examined Eurofer97/2 samples, submitted solely to preliminary thermal treatments, the SANS cross-sections are nearly coincident among each other and close to the one of Eurofer97/1, independently of austenitization or tempering temperature. An example is provided in Fig. 2, where the cross-sections of Eurofer97/1 submitted to standard treatment and of double austenitized Eurofer97/2 are compared. This is attributed to the fact that, in the absence of long term/high temperature ageing, the precipitate volume fraction is too low to produce significant SANS effects (that is lower than 0.0001 in order of magnitude), although some precipitates are certainly present and observable by SEM and TEM. Changes in grain size distribution, like those shown in Refs. [3,4] are generally not observable by this technique.

The Eurofer97/2 ausformed sample shows quite different features. First, its 2D SANS intensity distribution is significantly more anisotropic compared to Eurofer97/1, as shown in Fig. 3. The different orientation

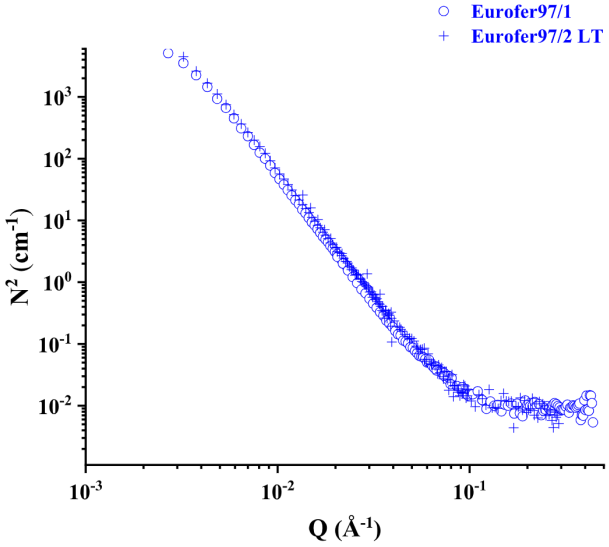

Fig. 2. Nuclear SANS cross-section for Eurofer97/1 reference heat 83697, 1040 °C 30′ + 750 °C 1.5 h measured at KWS-2 instrument (circles) and for LT Eurofer97/2 heat measured at KWS-1 instrument (crosses).

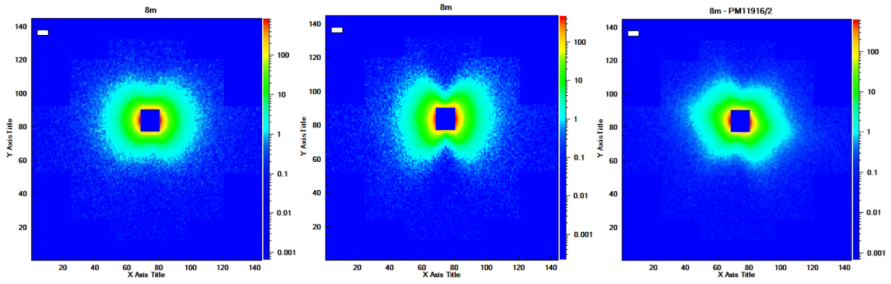

Fig. 3. 2D SANS pattern (neutron counts ranging from 0 to 10^3) measured for D = 8 m and λ = 5 Å for Eurofer97/1 reference heat 83697, 1040 °C 30′ + 750 °C 1.5 h (a), for Eurofer97/2 1175 °C 30′ + ausformed at 650 °C (b) and for Eurofer97/2 1175 °C 30′ + ausformed at 650 °C + 1 h 760 °C (c). The magnetic field direction is vertical in the plane of the figure.

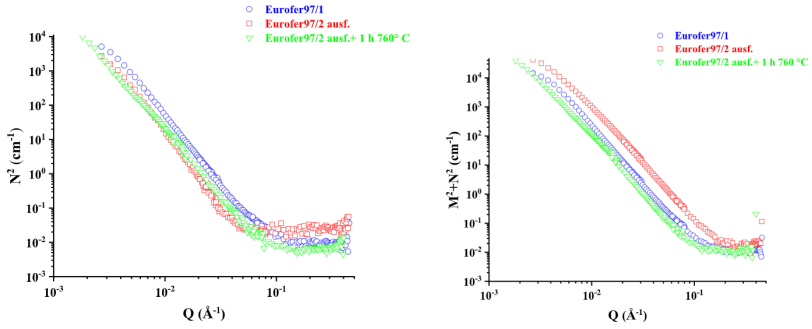

Fig. 4. Calibrated SANS cross-sections parallel (a) and perpendicular (b) to magnetic field for Eurofer97/1 reference heat 83697, 1040 °C 30′ + 750 °C 1.5 h (blue, circles), for Eurofer97/2 1175 °C 30′ + ausformed at 650 °C (red, squares) and for Eurofer97/2 1175 °C 30′ + ausformed at 650 °C + 1 h 760 °C (green, triangles). (For interpretation of the references to colour in this figure legend, the reader is referred to the web version of this article.)

of the "8-shaped" 2D intensity distribution pattern with respect to the applied magnetic field (vertical in the plane of the figure) is due to the fact that the ausformed ingots are textured and the two respective samples were not cut with the same orientation with respect to the rolling direction. Furthermore, the nuclear SANS components of these three samples are nearly coincident (Fig. 4 a) within the uncertainty associated to their different orientation, but the nuclear plus magnetic SANS component of the ausformed one is one order of magnitude higher compared to Eurofer97/1 and to Eurofer97/2 tempered after ausforming (Fig. 4 b). This reflects in the *R(Q)* ratio of the ausformed sample, compared in Fig. 5 with the Eurofer97/1 sample: for Eurofer97/2 ausformed *R(Q)* is nearly 10 times higher up to 0.1 $Å^{-1}$ approximately, then drops to same value range as Eurofer97/1.

The polarized SANS measurements were carried out on the ausformed sample and on the Eurofer97/2 sample submitted to double austenitization. Fig. 6 a – b shows the nuclear-magnetic interference term (Eq. (5)) measured for these two samples. Over all the investigated Q-range, such interference is always positive for non-ausformed Eurofer97/2. For the ausformed Eurofer97/2 it is negative down to a Q value corresponding to defect size of approximately 60 Å, then switches to positive value. This effect confirms the presence of a different magnetic micro-structure in the ausformed sample and provides an indication of the minimum size of the defects originating it. This behavior is also quite similar to the *R(Q)* one shown in Fig. 5. As discussed in Ref. [21], for Eurofer97/1 (or the LT sample) *R (Q)* is attributed to non-magnetic $M_{23}C_6$ carbides embedded in magnetic martensite. Since the chemical composition of Eurofer97/1 and Eurofer97/2 ausformed is basically the same, higher *R(Q)* for the latter implies for $Q < 0.1$ $Å^{-1}$ a higher magnetic contrast $(\Delta\rho)_{mag}^2$ and negative $(\Delta\rho)_{mag}$ since $NM < 0$ in that range.

The diffractograms of these three samples are shown in Fig. 7: with respect to the diffraction pattern of Eurofer97/1, two additional diffraction lines are present in the ausformed Eurofer97/2 sample and disappear after subsequent tempering. The lattice plane distances corresponding to these extra lines are 1.27 Å and 1.80 Å, coinciding with the (220) and (200) reflections of the austenite phase respectively [22]. Comparing the integrated intensity of the (200) peak of the austenite and of the alpha-Fe phase, whose form factors are nearly the same, gives an austenite volume fraction of 0.17 ± 0.02, obtained with a Gaussian fit and constant background. The presence of a non-

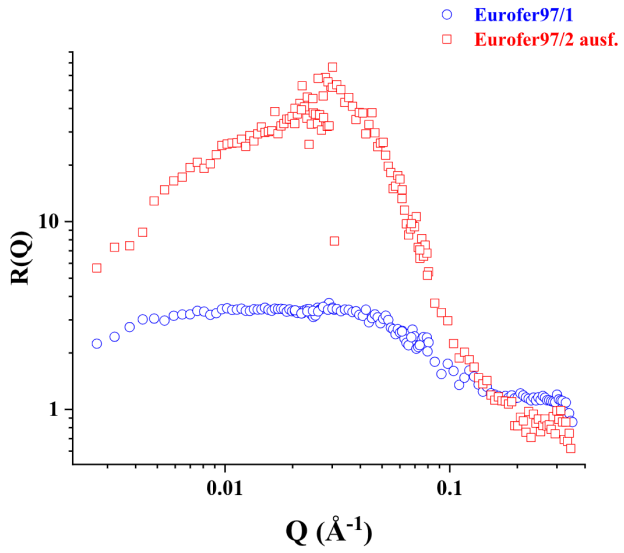

Fig. 5. *R(Q)* values for for Eurofer97/1 reference heat 83697, 1040 °C 30′ + 750 °C 1.5 h (blue, circles) and for Eurofer97/2 1175 °C 30′ + ausformed at 650 °C (red, squares). (For interpretation of the references to colour in this figure legend, the reader is referred to the web version of this article.)

magnetic phase, the austenite, embedded in the magnetic ferritic/martensitic matrix of the Eurofer97/2, provides a plausible explanation both of the stronger anisotropy in the 2D SANS pattern (Fig. 3) and of the anomalous magnetic SANS cross-section of this sample (Fig. 4 b). It also matches with the correlated behaviors of the *R(Q)* (Fig. 5) and of the nuclear-magnetic interference (Fig. 6). Although unmistakable in Fig. 7, this identification of the austenite phase in the ausformed Eurofer97/2 is a preliminary estimate and needs to be confirmed by neutron diffraction measurements covering a larger Q range, allowing for a refinement with an accurate estimate of the volume fractions for all the phases present in the sample. Also the sample tempered after ausforming should be investigated in this way to check whether a small volume fraction of austenite is still present: this would explain the strongly anisotropic 2D SANS pattern measured also for this sample (Fig. 3 c). It should also be mentioned that a previous polarized SANS study of a similar martensitic steel [16] has shown that negative nuclear-magnetic interference values can be associated to the presence of Fe-rich precipitates, namely of the Fe_3C phase. Certainly such

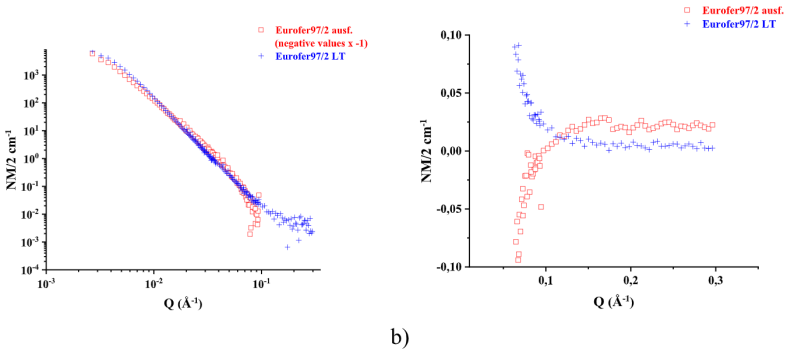

Fig. 6. Nuclear-magnetic interference for Eurofer97/2 heat LT (crosses, blue) and Eurofer97/2 1175 °C 30′ + ausformed at 650 °C (squares, red): a) full spectrum (negative values of ausformed sample multiplied by −1), b) magnification for $Q < 10^{-1}$ Å^{-1}. (For interpretation of the references to colour in this figure legend, the reader is referred to the web version of this article.)

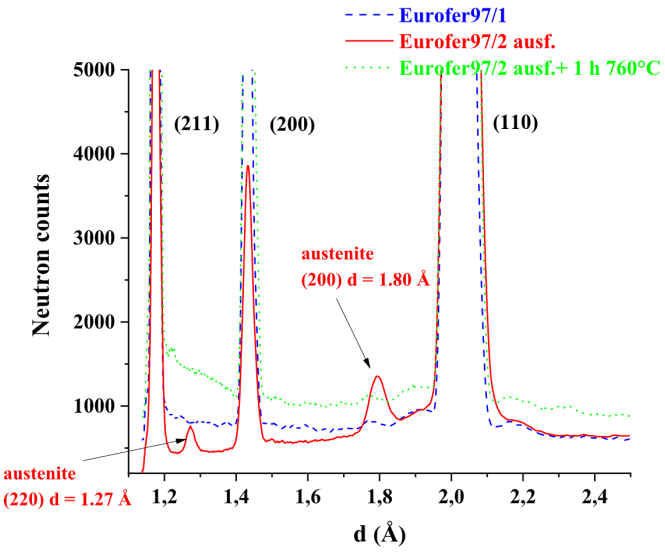

Fig. 7. Neutron diffractograms (normalized neutron counts vs lattice plane distance, in Å) for the same samples of Fig. 3: Eurofer97/1 reference heat 83697, 1040 °C 30′ + 750 °C 1.5 h (blue, dashed line), Eurofer97/2 1175 °C 30′ + ausformed at 650 °C (red, continuous line) and Eurofer97/2 1175 °C 30′ + ausformed at 650 °C + 1 h 760 °C (green, dotted line). Due to the low instrument resolution at 2.1 Å [20], the (1 1 1) austenite and (1 1 0) Eurofer97/2 peaks could not be separated. (For interpretation of the references to colour in this figure legend, the reader is referred to the web version of this article.)

precipitates have been observed in Eurofer97/2 after ausforming, but the available neutron diffraction data of Fig. 7 do not reveal any reflection to be reliably associated to such phases. Finally, dense dislocation networks have also been observed in thermo-mechanically treated Eurofer97 [23], but based on the current knowledge of the investigated problem they might not explain the observed SANS effects, requiring either compositional or magnetic differences between the defects and the matrix (see Section 3).

5. Conclusions

SANS has been utilized to try and contribute in understanding the correlation between micro-structural changes and mechanical properties in a series of Eurofer97/2 innovative heats. No SANS effects are observed when varying tempering or austenitization temperatures or also introducing a double austenitization (Fig. 2), independently of the heat elemental composition. Therefore, the changes observed in the mechanical properties of these heats should not be attributed to significant changes in precipitate composition or volume fractions, but to different micro-structural features, such as probably grain size. TEM work is in progress, particularly to check the presence of Fe-rich precipitates after ausforming and possibly identify their composition. Fig. 1 also shows that the SANS cross sections of these new Eurofer97/2 heats are identical to Eurofer97/1, at least for the investigated treatments.

Polarized SANS and neutron diffraction have provided a deeper insight into the micro-structural effects associated to ausforming in Eurofer97/2. Namely, there is strong evidence that a significant volume fraction of austenite is present in Eurofer97/2 just after ausforming and is mostly removed by the subsequent tempering. Although the material will be utilized in service only after tempering, it is important to monitor the changes in micro-structure and crystallographic phases during all the thermo-mechanical history of such a complex alloy; this is particularly relevant in view of understanding the still unknown irradiation behavior of the new Eurofer97/2 heats. Finally, it is stressed that the obtained results although preliminary constitute a unique contribution to understand the micro-structural effect of ausforming, obtainable by no other experimental method.

Declaration of Competing Interest

The authors declare that they have no known competing financial interests or personal relationships that could have appeared to influence the work reported in this paper.

Acknowledgements

This work has been carried out within the frame of the EUROfusion Consortium and has received funding from the Euratom research and training programme 2014–2018 and 2019-2020 under grant agreement No 633053. The views and opinions expressed herein do not necessarily reflect those of the European Commission. Dr. M. Hofmann (TUM) is gratefully acknowledged for suggesting the metallurgical interpretation of the neutron diffraction results. Dr. V. Pipinch (FZJ – JCNS) and Dr. G. Mangiapia (HZG) are acknowledged for help in handling the SANS data. Dr. R. Lindau (KIT) is acknowledged for providing the Eurofer97/1 sample.

References

[1] R.L. Klueh, A.T. Nelson, J. Nucl. Mat. 371 (2007) 37–52.
[2] G. Federici, W. Biel, M.R. Gilbert, R. Kemp, N. Taylor, N. Wenninger, European DEMO design strategies and consequences for materials, Nucl. Fusion 57 (2017) 092002.
[3] C. Cristalli, L. Pilloni, O. Tassa, L. Bozzetto, R. Sorci, L. Masotti, Development of innovative steels and thermo-mechanical treatments for DEMO high operating temperature blanket options, Nucl. Mater. Energy 16 (2018) 175–180.
[4] L. Pilloni, C. Cristalli, O. Tassa, I. Salvatori, S. Storai, Grain size reduction strategies on Eurofer, Nucl. Mater. Energy 17 (2018) 129–136.
[5] L. Pilloni, C. Cristalli, O. Tassa, L. Bozzetto, E. Zanin, N. Bettocchi, Development of innovative materials and thermal treatments for DEMO water cooled blanket, Nucl. Mater. Energy 19 (2019) 79–86.

[6] L. Tan, Y. Yan, J.T. Busby, Effects of alloying elements and thermomechanical treatment on 9Cr Reduced Activation Ferritic–Martensitic (RAFM) steels, J. Nucl. Mater. 442 (2013) S13–S17.
[7] A. Puype, L. Malerba, N. De Wispelaere, R. Petrov, J. Sietsma, Effect of processing on microstructural features and mechanical properties of a reduced activitation ferritic/martensitic EUROFER steel grade, J. Nucl. Mater. 494 (2017) 1–9.
[8] J. Hoffmann, M. Rieth, L. Commin, P. Fernández, M. Roldán, Improvement of reduced activation 9%Cr steels by ausforming, Nucl. Mater. Energy 6 (2016) 12–17.
[9] E. Piozin, Effect of thermomechanical treatments on the microstructure and mechanical properties of a 9%Cr martensitic steel (Grade 91), PhD Thesis, CEA-R-6402 report (2015).
[10] R. Coppola, D. Mirabile Gattia, L. Pilloni, Final Report EUROfusion Task WPMAT-2.2.3-T004-D002 ref. 2NPS4R Dec. 2019.
[11] R. Coppola, M. Klimenkov, Dose dependence of micro-voids distributions in low-temperature neutron irradiated Eurofer97 steel, Metals 9 (2019) 552.
[12] G. Kostorz, X-ray and neutron scattering, in: Physical Metallurgy, R.W. Cahn, P. Haasen, (Eds), North Holland, 1983. pp. 793–853.
[13] M.T. Hutchings, C.G. Windsor, in: K. Sköld, D.L. Price (Eds). Methods of Experimental Physics, vol 23-c, Neutron Scattering, Academic, 1987, pp. 405–482.
[14] A. Michels, Magnetic small-angle neutron scattering of bulk ferromagnets, J. Phys.: Condens. Matter 26 (38) (2014) 383201, https://doi.org/10.1088/0953-8984/26/38/383201.
[15] S. Mühlbauer, D. Honecker, É.A. Périgo, F. Bergner, S. Disch, A. Heinemann, S. Erokhin, D. Berkov, C. Leighton, M. Ring Eskildsen, A. Michels, Magnetic small-angle neutron scattering, Rev. Mod. Phys. 91 (2019) 015004.
[16] R. Coppola, R. Kampmann, M. Magnani, P. Staron, Microstructural characterization, using polarized neutron scattering, of a martensitic steel for fusion reactors, Acta Mat. 46 (1998) 5547–5556.
[17] R. Coppola, R. Lindau, M. Magnani, R.P. May, A. Möslang, M. Valli, Polarised SANS study of microstructural radiation damage in technical steels for nuclear applications, Phyisca B 385–386 (2006) 647–649.
[18] A. Radulescu, V. Pipich, H.M.-S. Frielinghaus, AppavouKWS-2, the high intensity / wide Q-range small-angle neutron diffractometer for soft-matter and biology at FRM II, J. Phys.: Conf. Ser. 351 (2012) 012026, , https://doi.org/10.1088/1742-6596/351/1/012026.
[19] A.V. Feoktystov, et al., KWS-1 high-resolution small-angle neutron scattering instrument at JCNS: current state, J. Appl. Cryst. 48 (1) (2015) 61–70, https://doi.org/10.1107/S1600576714025977.10.1107.
[20] Heinz Maier-Leibnitz Zentrum, et al., Diffuse scattering neutron time-of-flight spectrometer, Journal of large-scale research facilities 1 (2015) A27, https://doi.org/10.17815/jlsrf-1-33.
[21] R. Coppola, M. Klimenkov, R. Lindau, A. Möslang, M. Rieth, M. Valli, Microstructural effects of irradiation temperature and helium content in neutron irradiated B-alloyed Eurofer97-1 steel, Nucl. Mater. Energy 17 (2018) 40–47.
[22] http://www.icdd.com/downloadspatches/.
[23] M. Eddahbi, M.A. Mongea, T. Leguey, P. Fernández, R. Pareja, Texture and mechanical properties of EUROFER 97 steel processed by ECAP, Mater. Sci. Eng., A 528 (2011) 5927–5934.